Stellar Atmospheres: Lecture 12, 2020.06.04

Prof. Sundar Srinivasan

IRyA/UNAM

Final exam Mon/Tue

I will hand out graded homeworks and post solutions to the website over the weekend.

Relevant sections from books we used during the semester will also be available before the exam.

We will have a Zoom session Tuesday morning to address any doubts you may have.

References

1. Lamers & Casinelli, *Introduction to Stellar Winds*, Ch. 1-4, 7-8

Radiation-driven winds

Due to line (atoms and ions via resonance scattering) or continuum opacity (dust absorption/scattering) of materials.

Accleration due to radiation pressure $\propto \dfrac{L_* \overline{\kappa}}{4\pi r^2 c}$.

Radiation-driven winds

Due to line (atoms and ions via resonance scattering) or continuum opacity (dust absorption/scattering) of materials.

Accleration due to radiation pressure $\propto \dfrac{L_* \overline{\kappa}}{4\pi r^2 c}$. Eddington Factor $\Gamma \equiv \dfrac{\text{force due to radiation pressure}}{\text{force due to gravitational attraction}} = \dfrac{L_*}{M_*} \dfrac{\overline{\kappa}}{4\pi c G}$.

Γ is large for large $\dfrac{L_*}{M_*} \longrightarrow$ luminous cool giants and hot massive stars.

Radiation-driven winds

Due to line (atoms and ions via resonance scattering) or continuum opacity (dust absorption/scattering) of materials.

Accleration due to radiation pressure $\propto \frac{L_* \overline{\kappa}}{4\pi r^2 c}$. Eddington Factor $\Gamma \equiv \frac{\text{force due to radiation pressure}}{\text{force due to gravitational attraction}} = \frac{L_*}{M_*} \frac{\overline{\kappa}}{4\pi c G}$.

Γ is large for large $\frac{L_*}{M_*} \longrightarrow$ luminous cool giants and hot massive stars.

Line-driven winds

Hot massive stars (O, B).

$T \gtrsim 40\,000$ K, $L \gtrsim 10^5$ $L_\odot$.

$v_\infty \sim v_{\rm esc}(1.01R_*) \gtrsim 10^3$ km s^{-1}.

Appreciable Doppler shifts ($\sim 1\%$) that affect both line opacity and radiation field in the line.

Velocity gradient steep.

Dust-driven winds

Luminous cool giants (asymptotic giant branch, red supergiant).

$T \sim 2000 - 4000$ K, $L \sim 3000 - 10^5$ $L_\odot$.

$v_\infty \sim v_{\rm esc}(3R_*) \sim 10 - 30$ km s^{-1}.

Negligible Doppler shifts ($\sim 10^{-4}$; few Å), no change in continuum opacity or radiation field.

Comparatively shallow velocity gradient (acceleration zone more extended).

Eqn. of motion: isoth. stationary radiation-driven winds

For a purely pressure-driven wind, the Eddington Factor $\Gamma = 0$. Let us compare the results for this case with those for $\Gamma \neq 0$:

Eqn. of motion: isoth. stationary radiation-driven winds

For a purely pressure-driven wind, the Eddington Factor $\Gamma = 0$. Let us compare the results for this case with those for $\Gamma \neq 0$:

$F_{\rm rad}$ is inverse-square with magnitude $= \Gamma \times$ magnitude of grav. pull $\Longrightarrow$ modify gravitational term in equation of motion:

Eqn. of motion: isoth. stationary radiation-driven winds

For a purely pressure-driven wind, the Eddington Factor $\Gamma = 0$. Let us compare the results for this case with those for $\Gamma \neq 0$:

$F_{\rm rad}$ is inverse-square with magnitude $= \Gamma \times$ magnitude of grav. pull $\Longrightarrow$ modify gravitational term in equation of motion:

$$\frac{d \ln v}{dr} = \frac{\dfrac{2c_s^2}{r} - \dfrac{GM_*(1-\Gamma)}{r^2}}{v^2 - c_s^2}$$

Boundary condition: $\rho(r_0)$ is fixed. Velocity gradient, r_c, and MLR now depend on Γ.

Eqn. of motion: isoth. stationary radiation-driven winds

For a purely pressure-driven wind, the Eddington Factor $\Gamma = 0$. Let us compare the results for this case with those for $\Gamma \neq 0$:

$F_{\rm rad}$ is inverse-square with magnitude $= \Gamma \times$ magnitude of grav. pull $\Longrightarrow$ modify gravitational term in equation of motion:

$$\frac{d \ln v}{dr} = \frac{\frac{2c_s^2}{r} - \frac{GM_*(1-\Gamma)}{r^2}}{v^2 - c_s^2}$$

Boundary condition: $\rho(r_0)$ is fixed. Velocity gradient, r_c, and MLR now depend on Γ.

Case I: $\Gamma > 0$ for all $r > r_0$ (outward force exists everywhere in the acceleration zone, even in the subsonic regime)

Represents the situation for an ionised wind (radiation pressure due to electron scattering).

Eqn. of motion: isoth. stationary radiation-driven winds

For a purely pressure-driven wind, the Eddington Factor $\Gamma = 0$. Let us compare the results for this case with those for $\Gamma \neq 0$:

$F_{\rm rad}$ is inverse-square with magnitude $= \Gamma \times$ magnitude of grav. pull $\Longrightarrow$ modify gravitational term in equation of motion:

$$\frac{d \ln v}{dr} = \frac{\dfrac{2c_s^2}{r} - \dfrac{GM_*(1-\Gamma)}{r^2}}{v^2 - c_s^2}$$

Boundary condition: $\rho(r_0)$ is fixed. Velocity gradient, r_c, and MLR now depend on Γ.

Case I: $\Gamma > 0$ for all $r > r_0$ (outward force exists everywhere in the acceleration zone, even in the subsonic regime)

Represents the situation for an ionised wind (radiation pressure due to electron scattering).

$r_c(\Gamma) = \dfrac{GM_*}{2c_s^2}(1-\Gamma) = r_c(0)(1-\Gamma) < r_c(0)$, the value for a purely pressure-driven wind.

Eqn. of motion: isoth. stationary radiation-driven winds

For a purely pressure-driven wind, the Eddington Factor $\Gamma = 0$. Let us compare the results for this case with those for $\Gamma \neq 0$:

$F_{\rm rad}$ is inverse-square with magnitude $= \Gamma \times$ magnitude of grav. pull $\Longrightarrow$ modify gravitational term in equation of motion:

$$\frac{d \ln v}{dr} = \frac{\frac{2c_s^2}{r} - \frac{GM_*(1-\Gamma)}{r^2}}{v^2 - c_s^2}$$

Boundary condition: $\rho(r_0)$ is fixed. Velocity gradient, r_c, and MLR now depend on Γ.

Case I: $\Gamma > 0$ for all $r > r_0$ (outward force exists everywhere in the acceleration zone, even in the subsonic regime)

Represents the situation for an ionised wind (radiation pressure due to electron scattering).

$r_c(\Gamma) = \frac{GM_*}{2c_s^2}(1-\Gamma) = r_c(0)(1-\Gamma) < r_c(0)$, the value for a purely pressure-driven wind.

$\Gamma > 0 \Longrightarrow$, shallower velocity gradient than in the purely pressure-driven case $\Longrightarrow v(r_0)$ is higher (must reach c_s faster).

$\Longrightarrow$ since $\rho(r_0)$ is constant, $\dot{M}$ is higher than in the $\Gamma = 0$ case.

Eqn. of motion: isoth. stationary radiation-driven winds

For a purely pressure-driven wind, the Eddington Factor $\Gamma = 0$. Let us compare the results for this case with those for $\Gamma \neq 0$:

$F_{\rm rad}$ is inverse-square with magnitude $= \Gamma \times$ magnitude of grav. pull $\Longrightarrow$ modify gravitational term in equation of motion:

$$\frac{d \ln v}{dr} = \frac{\dfrac{2c_s^2}{r} - \dfrac{GM_*(1-\Gamma)}{r^2}}{v^2 - c_s^2}$$

Boundary condition: $\rho(r_0)$ is fixed. Velocity gradient, r_c, and MLR now depend on Γ.

Case I: $\Gamma > 0$ for all $r > r_0$ (outward force exists everywhere in the acceleration zone, even in the subsonic regime)

Represents the situation for an ionised wind (radiation pressure due to electron scattering).

$r_c(\Gamma) = \dfrac{GM_*}{2c_s^2}(1-\Gamma) = r_c(0)(1-\Gamma) < r_c(0)$, the value for a purely pressure-driven wind.

$\Gamma > 0 \Longrightarrow$, shallower velocity gradient than in the purely pressure-driven case $\Longrightarrow v(r_0)$ is higher (must reach c_s faster).

$\Longrightarrow$ since $\rho(r_0)$ is constant, $\dot{M}$ is higher than in the $\Gamma = 0$ case.

For an outflow, we need velocity gradient > 0 everywhere $\Rightarrow \Gamma < 1 - \dfrac{r_0}{r_c}$ in subsonic regime. Supersonic: Γ can be > 1.

Eqn. of motion: isoth. stationary radiation-driven winds

For a purely pressure-driven wind, the Eddington Factor $\Gamma = 0$. Let us compare the results for this case with those for $\Gamma \neq 0$:

$F_{\rm rad}$ is inverse-square with magnitude $= \Gamma \times$ magnitude of grav. pull $\implies$ modify gravitational term in equation of motion:

$$\frac{d \ln v}{dr} = \frac{\frac{2c_s^2}{r} - \frac{GM_*(1-\Gamma)}{r^2}}{v^2 - c_s^2}$$

Boundary condition: $\rho(r_0)$ is fixed. Velocity gradient, r_c, and MLR now depend on Γ.

Case I: $\Gamma > 0$ for all $r > r_0$ (outward force exists everywhere in the acceleration zone, even in the subsonic regime)

Represents the situation for an ionised wind (radiation pressure due to electron scattering).

$$r_c(\Gamma) = \frac{GM_*}{2c_s^2}(1-\Gamma) = r_c(0)(1-\Gamma) < r_c(0),$$ the value for a purely pressure-driven wind.

$\Gamma > 0 \implies$, shallower velocity gradient than in the purely pressure-driven case $\implies v(r_0)$ is higher (must reach c_s faster).

$\implies$ since $\rho(r_0)$ is constant, $\dot{M}$ is higher than in the $\Gamma = 0$ case.

For an outflow, we need velocity gradient > 0 everywhere $\Rightarrow \Gamma < 1 - \frac{r_0}{r_c}$ in subsonic regime. Supersonic: Γ can be > 1.

Case II: $\Gamma > 0$ for $r > r_d > r_0$ (outward force "turns on" somewhere inside the acceleration zone)

Represents the situation for a dust-driven wind, with r_d the dust-formation radius.

Eqn. of motion: isoth. stationary radiation-driven winds

For a purely pressure-driven wind, the Eddington Factor $\Gamma = 0$. Let us compare the results for this case with those for $\Gamma \neq 0$:

$F_{\rm rad}$ is inverse-square with magnitude $= \Gamma \times$ magnitude of grav. pull $\Longrightarrow$ modify gravitational term in equation of motion:

$$\frac{d \ln v}{dr} = \frac{\dfrac{2c_s^2}{r} - \dfrac{GM_*(1-\Gamma)}{r^2}}{v^2 - c_s^2}$$

Boundary condition: $\rho(r_0)$ is fixed. Velocity gradient, r_c, and MLR now depend on Γ.

Case I: $\Gamma > 0$ for all $r > r_0$ (outward force exists everywhere in the acceleration zone, even in the subsonic regime)

Represents the situation for an ionised wind (radiation pressure due to electron scattering).

$r_c(\Gamma) = \dfrac{GM_*}{2c_s^2}(1-\Gamma) = r_c(0)(1-\Gamma) < r_c(0)$, the value for a purely pressure-driven wind.

$\Gamma > 0 \Longrightarrow$, shallower velocity gradient than in the purely pressure-driven case $\Longrightarrow v(r_0)$ is higher (must reach c_s faster).

$\Longrightarrow$ since $\rho(r_0)$ is constant, $\dot{M}$ is higher than in the $\Gamma = 0$ case.

For an outflow, we need velocity gradient > 0 everywhere $\Rightarrow \Gamma < 1 - \dfrac{r_0}{r_c}$ in subsonic regime. Supersonic: Γ can be > 1.

Case II: $\Gamma > 0$ for $r > r_d > r_0$ (outward force "turns on" somewhere inside the acceleration zone)

Represents the situation for a dust-driven wind, with r_d the dust-formation radius.

II a: $r_d > r_c(\Gamma)$: the subsonic structure (velocity/density gradient, MLR) is unaffected. $r_c = r_c(0)(1-\Gamma)$.

Beyond r_d, the velocity gradient is higher, so v_∞ is higher than in the purely pressure-driven case.

Eqn. of motion: isoth. stationary radiation-driven winds

For a purely pressure-driven wind, the Eddington Factor $\Gamma = 0$. Let us compare the results for this case with those for $\Gamma \neq 0$:

$F_{\rm rad}$ is inverse-square with magnitude $= \Gamma \times$ magnitude of grav. pull $\Longrightarrow$ modify gravitational term in equation of motion:

$$\frac{d \ln v}{dr} = \frac{\frac{2c_s^2}{r} - \frac{GM_*(1-\Gamma)}{r^2}}{v^2 - c_s^2}$$

Boundary condition: $\rho(r_0)$ is fixed. Velocity gradient, r_c, and MLR now depend on Γ.

Case I: $\Gamma > 0$ for all $r > r_0$ (outward force exists everywhere in the acceleration zone, even in the subsonic regime)

Represents the situation for an ionised wind (radiation pressure due to electron scattering).

$r_c(\Gamma) = \frac{GM_*}{2c_s^2}(1-\Gamma) = r_c(0)(1-\Gamma) < r_c(0)$, the value for a purely pressure-driven wind.

$\Gamma > 0 \Longrightarrow$, shallower velocity gradient than in the purely pressure-driven case $\Longrightarrow v(r_0)$ is higher (must reach c_s faster).

$\Longrightarrow$ since $\rho(r_0)$ is constant, $\dot{M}$ is higher than in the $\Gamma = 0$ case.

For an outflow, we need velocity gradient > 0 everywhere $\Rightarrow \Gamma < 1 - \frac{r_0}{r_c}$ in subsonic regime. Supersonic: Γ can be > 1.

Case II: $\Gamma > 0$ for $r > r_d > r_0$ (outward force "turns on" somewhere inside the acceleration zone)

Represents the situation for a dust-driven wind, with r_d the dust-formation radius.

II a: $r_d > r_c(\Gamma)$: the subsonic structure (velocity/density gradient, MLR) is unaffected. $r_c = r_c(0)(1-\Gamma)$.

Beyond r_d, the velocity gradient is higher, so v_∞ is higher than in the purely pressure-driven case.

II b: $r_d < r_c(\Gamma)$: velocity gradient suddenly becomes shallower in the subsonic regime beyond r_d, MLR $>$ in the $\Gamma = 0$ case.

$r_c \approx r_d$, in the region where Γ suddenly changes.

Dust-driven winds in cool stars

$$L_{\rm Edd} \approx 3.2 \times 10^4 \left(\frac{M}{\rm M_\odot}\right) \left(\frac{\overline{\kappa}}{0.039\ \rm m^2\ kg^{-1}}\right)^{-1} \rm L_\odot;\ \overline{\kappa}_{\rm dust} \sim 0.3 - 1.0\ m^2\ kg^{-1} \implies L_{\rm Edd} \approx 3000 \left(\frac{M}{\rm M_\odot}\right) \rm L_\odot.$$

Dust-driven winds in cool stars

$$L_{\rm Edd} \approx 3.2 \times 10^4 \left(\frac{M}{\rm M_\odot}\right) \left(\frac{\overline{\kappa}}{0.039\ {\rm m^2\ kg^{-1}}}\right)^{-1} {\rm L_\odot};\ \overline{\kappa}_{\rm dust} \sim 0.3 - 1.0\ {\rm m^2\ kg^{-1}} \Longrightarrow L_{\rm Edd} \approx 3000 \left(\frac{M}{\rm M_\odot}\right) {\rm L_\odot}.$$

Need pulsations to levitate gas to cooler regions to form dust. Semi-regular variables (small amplitude, $P < 100$ d), long-period variables (large amplitude, fundamental mode, $P \sim 100 - 300$ d). Mira-type stars are LPVs. Pulsations also drive a weak wind.

Dust-driven winds in cool stars

$$L_{\rm Edd} \approx 3.2 \times 10^4 \left(\frac{M}{{\rm M}_\odot}\right) \left(\frac{\overline{\kappa}}{0.039\ {\rm m}^2\ {\rm kg}^{-1}}\right)^{-1} {\rm L}_\odot;\ \overline{\kappa}_{\rm dust} \sim 0.3 - 1.0\ {\rm m}^2\ {\rm kg}^{-1} \implies L_{\rm Edd} \approx 3000 \left(\frac{M}{{\rm M}_\odot}\right) {\rm L}_\odot.$$

Need pulsations to levitate gas to cooler regions to form dust. Semi-regular variables (small amplitude, $P < 100$ d), long-period variables (large amplitude, fundamental mode, $P \sim 100 - 300$ d). Mira-type stars are LPVs. Pulsations also drive a weak wind.

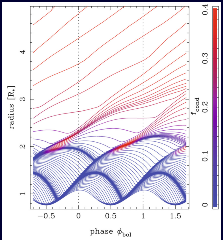

Nowotny et al. 2010 A&A 514, A35

Gas layers levitated by pulsations travel on ballistic trajectories to cooler regions ($R \sim 1.5 - 3R_*$, $T \lesssim 1800$ K) where they condense into solid particles (dust), whose higher κ immediately drives a strong outflow. The dust drags the gas along with it.

$$L_{\rm Edd} \approx 3.2 \times 10^4 \left(\frac{M}{\rm M_\odot}\right)\left(\frac{\overline{\kappa}}{0.039~{\rm m^2~kg^{-1}}}\right)^{-1} {\rm L_\odot};\ \overline{\kappa}_{\rm dust} \sim 0.3 - 1.0~{\rm m^2~kg^{-1}} \implies L_{\rm Edd} \approx 3000 \left(\frac{M}{\rm M_\odot}\right) {\rm L_\odot}.$$

Need pulsations to levitate gas to cooler regions to form dust. Semi-regular variables (small amplitude, $P < 100$ d), long-period variables (large amplitude, fundamental mode, $P \sim 100 - 300$ d). Mira-type stars are LPVs. Pulsations also drive a weak wind.

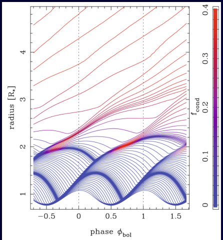

Nowotny et al. 2010 A&A 514, A35

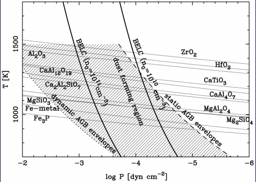

Elvis et al. 2002 ApJ 567, L107

Gas layers levitated by pulsations travel on ballistic trajectories to cooler regions ($R \sim 1.5 - 3R_*$, $T \lesssim 1800$ K) where they condense into solid particles (dust), whose higher κ immediately drives a strong outflow. The dust drags the gas along with it.

AGB star atmospheres start out oxygen-rich. Stars with masses $2 - 4~{\rm M_\odot}$ become carbon-rich by the third dredge-up process. The chemistry of the molecules and dust in the envelope is regulated accordingly.

O-rich dust: refractory oxides (Al, Mg), amorphous silicates (olivine, pyroxene), crystalline silicates (enstatite).

C-rich dust: amorphous carbon, diamond/graphite, silicon carbide, MgS, hydrogenated amorphous carbons (HACs).

$$L_{\rm Edd} \approx 3.2 \times 10^4 \left(\frac{M}{\rm M_\odot}\right)\left(\frac{\overline{\kappa}}{0.039\ {\rm m^2\ kg^{-1}}}\right)^{-1} {\rm L_\odot};\ \overline{\kappa}_{\rm dust} \sim 0.3 - 1.0\ {\rm m^2\ kg^{-1}} \Longrightarrow L_{\rm Edd} \approx 3000 \left(\frac{M}{\rm M_\odot}\right) {\rm L_\odot}.$$

Need pulsations to levitate gas to cooler regions to form dust. Semi-regular variables (small amplitude, $P < 100$ d), long-period variables (large amplitude, fundamental mode, $P \sim 100 - 300$ d). Mira-type stars are LPVs. Pulsations also drive a weak wind.

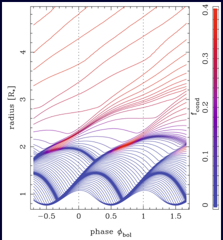

Nowotny et al. 2010 A&A 514, A35

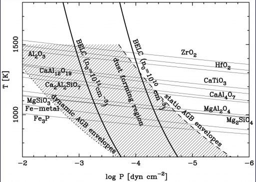

Elvis et al. 2002 ApJ 567, L107

Gas layers levitated by pulsations travel on ballistic trajectories to cooler regions ($R \sim 1.5 - 3R_*$, $T \lesssim 1800$ K) where they condense into solid particles (dust), whose higher κ immediately drives a strong outflow. The dust drags the gas along with it.

AGB star atmospheres start out oxygen-rich. Stars with masses $2 - 4\ {\rm M_\odot}$ become carbon-rich by the third dredge-up process. The chemistry of the molecules and dust in the envelope is regulated accordingly.

O-rich dust: refractory oxides (Al, Mg), amorphous silicates (olivine, pyroxene), crystalline silicates (enstatite).

C-rich dust: amorphous carbon, diamond/graphite, silicon carbide, MgS, hydrogenated amorphous carbons (HACs).

The MLR depends on the chemistry – in general, carbonaceous dust has higher κ and hence is more efficient in absorbing radiation. Silicate dust requires iron to enhance its opacity (*e.g.*, Höfner 2007 ASPC 378, 145).

Line-driven winds in hot stars

UV/X-ray resonance lines of highly ionised species $\underbrace{\text{C II, Fe II, Mg II}}_{\sim 10\text{ eV},\, T_{\rm eff} \sim 20\,000\text{ K}}, \cdots, \underbrace{\text{N V, O VI}}_{\sim 100\text{ eV},\, T_{\rm eff} \sim 50\,000\text{ K}}$

Line-driven winds in hot stars

UV/X-ray resonance lines of highly ionised species $\underbrace{\text{C II, Fe II, Mg II}}_{\sim 10\text{ eV},\, T_{\rm eff} \sim 20\,000\text{ K}}, \cdots, \underbrace{\text{N V, O VI}}_{\sim 100\text{ eV},\, T_{\rm eff} \sim 50\,000\text{ K}}$

Consider a resonance line with energy $h\nu_0$.

Near the photosphere, $v(r_0) \ll v_\infty$, ions absorb photons of rest frequency $\nu = \nu_0$.

As $r \uparrow$, $v(r) \uparrow$ (outflow). Ions at $r \gg r_0$ absorb photons with rest frequency $\nu = \nu_0(1 + v_\infty/c)$.

Thermal broadening of resonance line: $\Delta\nu_D \approx \frac{c_s}{c}\nu_0 \approx 10^{-6}\nu_0$.

Range of rest frequencies absorbed in acceleration zone: $\Delta\nu_{\rm W} \approx \frac{v_\infty}{c}\nu_0 \approx 3 \times 10^{-3}\nu_0 \gg \Delta\nu_D$.

Thus, ions everywhere in the acceleration zone have unabsorbed photons available in their respective frequency range.

Line-driven winds in hot stars

UV/X-ray resonance lines of highly ionised species $\underbrace{\text{C II, Fe II, Mg II}}_{\sim 10\text{ eV}, T_{\text{eff}} \sim 20\,000\text{ K}}, \cdots, \underbrace{\text{N V, O VI}}_{\sim 100\text{ eV}, T_{\text{eff}} \sim 50\,000\text{ K}}$

Consider a resonance line with energy $h\nu_0$.

Near the photosphere, $v(r_0) \ll v_\infty$, ions absorb photons of rest frequency $\nu = \nu_0$.

As $r \uparrow$, $v(r) \uparrow$ (outflow). Ions at $r \gg r_0$ absorb photons with rest frequency $\nu = \nu_0(1 + v_\infty/c)$.

Thermal broadening of resonance line: $\Delta\nu_D \approx \frac{c_s}{c}\nu_0 \approx 10^{-6}\nu_0$.

Range of rest frequencies absorbed in acceleration zone: $\Delta\nu_{\text{W}} \approx \frac{v_\infty}{c}\nu_0 \approx 3 \times 10^{-3}\nu_0 \gg \Delta\nu_D$.

Thus, ions everywhere in the acceleration zone have unabsorbed photons available in their respective frequency range.

Momentum transfer rate for one line: $\dot{M}v_\infty \approx \frac{4\pi r^2}{c} \int_{\nu_0}^{\nu_0(1+v_\infty/c)} F_\nu \, d\nu \approx \frac{4\pi r^2}{c} F_{\nu_0} \nu_0 \frac{v_\infty}{c} \implies \dot{M} \approx \frac{L}{c^2}$

Line-driven winds in hot stars

UV/X-ray resonance lines of highly ionised species $\underbrace{\text{C II, Fe II, Mg II}}_{\sim 10\text{ eV},\, T_{\rm eff}\sim 20\,000\text{ K}}, \cdots, \underbrace{\text{N V, O VI}}_{\sim 100\text{ eV},\, T_{\rm eff}\sim 50\,000\text{ K}}$

Consider a resonance line with energy $h\nu_0$.

Near the photosphere, $v(r_0) \ll v_\infty$, ions absorb photons of rest frequency $\nu = \nu_0$.

As $r\uparrow$, $v(r)\uparrow$ (outflow). Ions at $r \gg r_0$ absorb photons with rest frequency $\nu = \nu_0(1 + v_\infty/c)$.

Thermal broadening of resonance line: $\Delta\nu_D \approx \frac{c_s}{c}\nu_0 \approx 10^{-6}\nu_0$.

Range of rest frequencies absorbed in acceleration zone: $\Delta\nu_{\rm W} \approx \frac{v_\infty}{c}\nu_0 \approx 3\times 10^{-3}\nu_0 \gg \Delta\nu_D$.

Thus, ions everywhere in the acceleration zone have unabsorbed photons available in their respective frequency range.

Momentum transfer rate for one line: $\dot{M}v_\infty \approx \frac{4\pi r^2}{c}\int_{\nu_0}^{\nu_0(1+v_\infty/c)} F_\nu\, d\nu \approx \frac{4\pi r^2}{c} F_{\nu_0}\nu_0 \frac{v_\infty}{c} \implies \dot{M} \approx \frac{L}{c^2}$

Multiple non-overlapping lines: $\dot{M} = N_{\rm eff}\frac{L}{c^2}$, where $N_{\rm eff}$ = Effective #(optically thick lines) $\equiv \frac{1}{\int_0^\infty F_\nu\, d\nu}\sum_{i=1}^{N}\int_{\nu_i}^{\nu_i(1+v_\infty/c)} F_\nu\, d\nu$.

Line-driven winds in hot stars

UV/X-ray resonance lines of highly ionised species $\underbrace{\text{C II, Fe II, Mg II}}_{\sim 10\text{ eV},\, T_{\rm eff}\sim 20\,000\text{ K}}, \cdots, \underbrace{\text{N V, O VI}}_{\sim 100\text{ eV},\, T_{\rm eff}\sim 50\,000\text{ K}}$

Consider a resonance line with energy $h\nu_0$.

Near the photosphere, $v(r_0) \ll v_\infty$, ions absorb photons of rest frequency $\nu = \nu_0$.

As $r \uparrow$, $v(r) \uparrow$ (outflow). Ions at $r \gg r_0$ absorb photons with rest frequency $\nu = \nu_0(1 + v_\infty/c)$.

Thermal broadening of resonance line: $\Delta\nu_D \approx \frac{c_s}{c}\nu_0 \approx 10^{-6}\nu_0$.

Range of rest frequencies absorbed in acceleration zone: $\Delta\nu_{\rm W} \approx \frac{v_\infty}{c}\nu_0 \approx 3\times 10^{-3}\nu_0 \gg \Delta\nu_D$.

Thus, ions everywhere in the acceleration zone have unabsorbed photons available in their respective frequency range.

Momentum transfer rate for one line: $\dot{M}v_\infty \approx \frac{4\pi r^2}{c}\int_{\nu_0}^{\nu_0(1+v_\infty/c)} F_\nu\, d\nu \approx \frac{4\pi r^2}{c}F_{\nu_0}\nu_0\frac{v_\infty}{c} \implies \dot{M} \approx \frac{L}{c^2}$

Multiple non-overlapping lines: $\dot{M} = N_{\rm eff}\frac{L}{c^2}$, where $N_{\rm eff}$ = Effective #(optically thick lines) $\equiv \frac{1}{\int_0^\infty F_\nu\, d\nu}\sum_{i=1}^{N}\int_{\nu_i}^{\nu_i(1+v_\infty/c)} F_\nu\, d\nu$.

Momentum fraction transferred to lines: $\frac{\dot{M}v_\infty}{L_*/c} \approx N_{\rm eff}\frac{v_\infty}{c} < 1$ (required) $\implies N_{\rm eff} < \frac{c}{v_\infty}$ (single-scattering limit).

Line-driven winds in hot stars

UV/X-ray resonance lines of highly ionised species $\underbrace{\text{C II, Fe II, Mg II}}_{\sim 10\text{ eV},\, T_{\rm eff} \sim 20\,000\text{ K}}, \cdots, \underbrace{\text{N V, O VI}}_{\sim 100\text{ eV},\, T_{\rm eff} \sim 50\,000\text{ K}}$

Consider a resonance line with energy $h\nu_0$.

Near the photosphere, $v(r_0) \ll v_\infty$, ions absorb photons of rest frequency $\nu = \nu_0$.

As $r \uparrow$, $v(r) \uparrow$ (outflow). Ions at $r \gg r_0$ absorb photons with rest frequency $\nu = \nu_0(1 + v_\infty/c)$.

Thermal broadening of resonance line: $\Delta\nu_D \approx \frac{c_s}{c}\nu_0 \approx 10^{-6}\nu_0$.

Range of rest frequencies absorbed in acceleration zone: $\Delta\nu_W \approx \frac{v_\infty}{c}\nu_0 \approx 3 \times 10^{-3}\nu_0 \gg \Delta\nu_D$.

Thus, ions everywhere in the acceleration zone have unabsorbed photons available in their respective frequency range.

Momentum transfer rate for one line: $\dot{M}v_\infty \approx \frac{4\pi r^2}{c}\int_{\nu_0}^{\nu_0(1+v_\infty/c)} F_\nu\, d\nu \approx \frac{4\pi r^2}{c} F_{\nu_0}\nu_0 \frac{v_\infty}{c} \implies \dot{M} \approx \frac{L}{c^2}$

Multiple non-overlapping lines: $\dot{M} = N_{\rm eff}\frac{L}{c^2}$, where $N_{\rm eff}$ = Effective #(optically thick lines) $\equiv \frac{1}{\int_0^\infty F_\nu\, d\nu}\sum_{i=1}^{N}\int_{\nu_i}^{\nu_i(1+v_\infty/c)} F_\nu\, d\nu$.

Momentum fraction transferred to lines: $\frac{\dot{M}v_\infty}{L_*/c} \approx N_{\rm eff}\frac{v_\infty}{c} < 1$ (required) $\implies N_{\rm eff} < \frac{c}{v_\infty}$ (single-scattering limit).

In dense winds (e.g., Wolf-Rayet stars), photons can successively scatter off of multiple ions/lines. MLR is enhanced.

Absolute limit: $\frac{1}{2}\dot{M}v_\infty^2 < L_* \implies \dot{M} \lesssim \frac{L_*}{v_\infty^2} \implies N_{\rm eff} < \left(\frac{c}{v_\infty}\right)^2 \sim 10^4$.

Wind diagnostics: P Cygni profiles - I

Result of isotropic resonance scattering by circumstellar material moving at different velocities w.r.t. observer.

Material in front of star produces strong absorption due to isothermal scattering. Weaker emission due to photons being scattered *into* line of sight (LOS). Absorption component is blue-shifted because material in front of star is approaching observer. Emission component arises from all parts of star, so covers almost whole range of velocities (except for the part originating from the region occulted by the stellar disk).

Wind diagnostics: P Cygni profiles - I

Result of isotropic resonance scattering by circumstellar material moving at different velocities w.r.t. observer.

Material in front of star produces strong absorption due to isothermal scattering. Weaker emission due to photons being scattered *into* line of sight (LOS). Absorption component is blue-shifted because material in front of star is approaching observer. Emission component arises from all parts of star, so covers almost whole range of velocities (except for the part originating from the region occulted by the stellar disk).

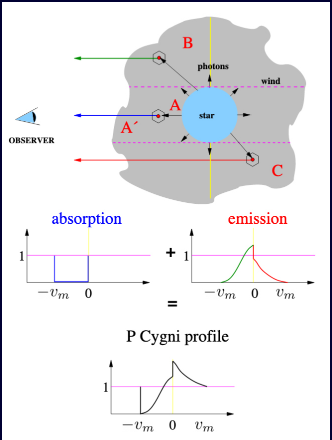

J. Puls, University Observatory Munich

Wind diagnostics: P Cygni profiles - I

Result of isotropic resonance scattering by circumstellar material moving at different velocities w.r.t. observer.

Material in front of star produces strong absorption due to isothermal scattering. Weaker emission due to photons being scattered *into* line of sight (LOS). Absorption component is blue-shifted because material in front of star is approaching observer. Emission component arises from all parts of star, so covers almost whole range of velocities (except for the part originating from the region occulted by the stellar disk).

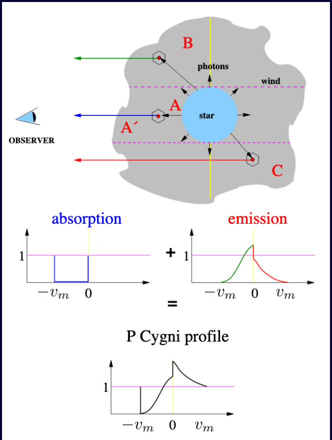

J. Puls, University Observatory Munich

$v \uparrow$ with r, $\rho \downarrow$. v_m is the maximum velocity ($< v_\infty$) at which a significant density of absorbing ions exists. As $\tau \uparrow$, $v_m \rightarrow v_\infty$.

Wind diagnostics: P Cygni profiles - I

Result of isotropic resonance scattering by circumstellar material moving at different velocities w.r.t. observer.

Material in front of star produces strong absorption due to isothermal scattering. Weaker emission due to photons being scattered *into* line of sight (LOS). Absorption component is blue-shifted because material in front of star is approaching observer. Emission component arises from all parts of star, so covers almost whole range of velocities (except for the part originating from the region occulted by the stellar disk).

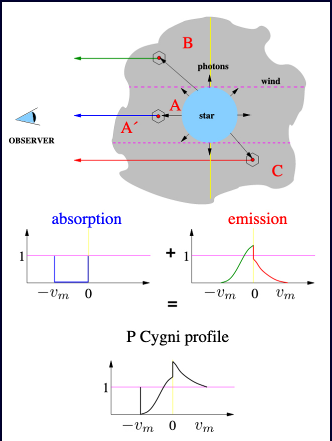

J. Puls, University Observatory Munich

$v \uparrow$ with r, $\rho \downarrow$. v_m is the maximum velocity ($< v_\infty$) at which a significant density of absorbing ions exists. As $\tau \uparrow$, $v_m \rightarrow v_\infty$.

Absorption profile:

Part A in the wind produces an absorption trough as it is in front of the stellar disk. Material from this region is approaching the observer, so the trough is blue-shifted. There is no corresponding red-shifted component as it is occulted by the stellar disk.

The profile is unsaturated if the residual flux is not zero. This can happen because there is always some emission along the LOS due to isotropic scattering.

Wind diagnostics: P Cygni profiles - I

Result of isotropic resonance scattering by circumstellar material moving at different velocities w.r.t. observer.

Material in front of star produces strong absorption due to isothermal scattering. Weaker emission due to photons being scattered *into* line of sight (LOS). Absorption component is blue-shifted because material in front of star is approaching observer. Emission component arises from all parts of star, so covers almost whole range of velocities (except for the part originating from the region occulted by the stellar disk).

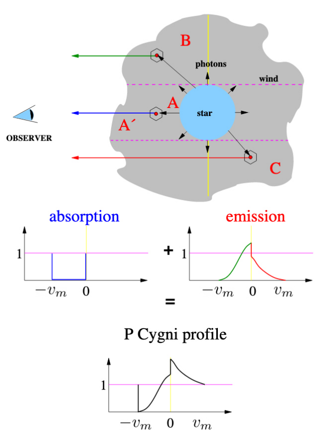

J. Puls, University Observatory Munich

$v \uparrow$ with r, $\rho \downarrow$. v_m is the maximum velocity ($< v_\infty$) at which a significant density of absorbing ions exists. As $\tau \uparrow$, $v_m \to v_\infty$.

Absorption profile:

Part A in the wind produces an absorption trough as it is in front of the stellar disk. Material from this region is approaching the observer, so the trough is blue-shifted. There is no corresponding red-shifted component as it is occulted by the stellar disk.

The profile is unsaturated if the residual flux is not zero. This can happen because there is always some emission along the LOS due to isotropic scattering. Emission profile:

Unlike absorption, emission arises from all parts of the star at all velocity components. It is not as strong as the absorption because the emission is isotropic (only a small chunk is directed towards the observer).

Wind diagnostics: P Cygni profiles - I

Result of isotropic resonance scattering by circumstellar material moving at different velocities w.r.t. observer.

Material in front of star produces strong absorption due to isothermal scattering. Weaker emission due to photons being scattered *into* line of sight (LOS). Absorption component is blue-shifted because material in front of star is approaching observer. Emission component arises from all parts of star, so covers almost whole range of velocities (except for the part originating from the region occulted by the stellar disk).

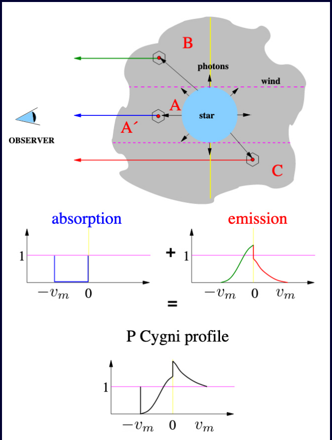

J. Puls, University Observatory Munich

$v \uparrow$ with r, $\rho \downarrow$. v_m is the maximum velocity ($< v_\infty$) at which a significant density of absorbing ions exists. As $\tau \uparrow$, $v_m \rightarrow v_\infty$.

Absorption profile:

Part A in the wind produces an absorption trough as it is in front of the stellar disk. Material from this region is approaching the observer, so the trough is blue-shifted. There is no corresponding red-shifted component as it is occulted by the stellar disk.

The profile is unsaturated if the residual flux is not zero. This can happen because there is always some emission along the LOS due to isotropic scattering. Emission profile:

Unlike absorption, emission arises from all parts of the star at all velocity components. It is not as strong as the absorption because the emission is isotropic (only a small chunk is directed towards the observer).

Part A' produces blue-shifted emission. The forward side-lobes in Part B scatter photons into the LOS of the observer. This is also blue-shifted as the region is part of the hemisphere that is approaching the observer.

Wind diagnostics: P Cygni profiles - I

Result of isotropic resonance scattering by circumstellar material moving at different velocities w.r.t. observer.

Material in front of star produces strong absorption due to isothermal scattering. Weaker emission due to photons being scattered *into* line of sight (LOS). Absorption component is blue-shifted because material in front of star is approaching observer. Emission component arises from all parts of star, so covers almost whole range of velocities (except for the part originating from the region occulted by the stellar disk).

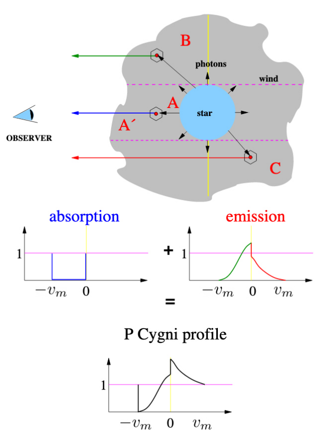

J. Puls, University Observatory Munich

$v \uparrow$ with r, $\rho \downarrow$. v_m is the maximum velocity ($< v_\infty$) at which a significant density of absorbing ions exists. As $\tau \uparrow$, $v_m \to v_\infty$.

Absorption profile:

Part A in the wind produces an absorption trough as it is in front of the stellar disk. Material from this region is approaching the observer, so the trough is blue-shifted. There is no corresponding red-shifted component as it is occulted by the stellar disk.

The profile is unsaturated if the residual flux is not zero. This can happen because there is always some emission along the LOS due to isotropic scattering. Emission profile:

Unlike absorption, emission arises from all parts of the star at all velocity components. It is not as strong as the absorption because the emission is isotropic (only a small chunk is directed towards the observer).

Part A' produces blue-shifted emission. The forward side-lobes in Part B scatter photons into the LOS of the observer. This is also blue-shifted as the region is part of the hemisphere that is approaching the observer.

Part C contains the backward side-lobes, which are receding from the observer. It contributes to the red-shifted part of the emission profile.

The emission is asymmetric because the central part of region C is occulted by the star.

Wind diagnostics: P Cygni profiles - II

1. Terminal velocity – if enough absorbing ions exist everywhere in the wind, absorption occurs at all velocities up to and including v_∞. If the blue edge is $\Delta\nu$ away from the central frequency ν_0, then $v_\infty = \frac{\Delta\nu}{\nu_0} c$.
2. Ion density – For an unsaturated profile, can generate theoretical profiles for various ion densities until we reproduce observed profile.
3. Shape of velocity field – Vary the theoretical velocity law and compute theoretical profiles until we reproduce observations.

Wind diagnostics: Hα profiles

Can determine MLR in hot stars. Hα is one of the strongest lines, so robust proxy for wind density. Well-understood behaviour.

Wind diagnostics: Hα profiles

Can determine MLR in hot stars. Hα is one of the strongest lines, so robust proxy for wind density. Well-understood behaviour.

Resonance lines: transitions between ground state and first excited state. Opacity $\propto$ ion density and density of radiation field.
Hα: Transition between excited ionisation states.

Wind diagnostics: Hα profiles

Can determine MLR in hot stars. Hα is one of the strongest lines, so robust proxy for wind density. Well-understood behaviour.

Resonance lines: transitions between ground state and first excited state. Opacity $\propto$ ion density and density of radiation field.

Hα: Transition between excited ionisation states. HII is the major ionisation stage for hydrogen in hot stars, can assume complete ionisation, and therefore $n_e \propto \rho$.

Wind diagnostics: Hα profiles

Can determine MLR in hot stars. Hα is one of the strongest lines, so robust proxy for wind density. Well-understood behaviour.

Resonance lines: transitions between ground state and first excited state. Opacity $\propto$ ion density and density of radiation field.

Hα: Transition between excited ionisation states. HII is the major ionisation stage for hydrogen in hot stars, can assume complete ionisation, and therefore $n_e \propto \rho$.

Wind diagnostics: Hα profiles

Can determine MLR in hot stars. Hα is one of the strongest lines, so robust proxy for wind density. Well-understood behaviour.

Resonance lines: transitions between ground state and first excited state. Opacity $\propto$ ion density and density of radiation field.

Hα: Transition between excited ionisation states. HII is the major ionisation stage for hydrogen in hot stars, can assume complete ionisation, and therefore $n_e \propto \rho$. Saha Equation for ionisation states $j, j+1$ and electronic state $\ell > 1$: $n_{\ell,j} \propto n_e n_{\ell,j+1} \propto \rho^2$.

The optical depth in the line is $\propto \alpha$, the absorption coefficient. $\alpha = n_{\mathrm{H}}\sigma \quad \propto n_e n_{\mathrm{HII}} \propto \rho^2$.

Wind diagnostics: Hα profiles

Can determine MLR in hot stars. Hα is one of the strongest lines, so robust proxy for wind density. Well-understood behaviour.

Resonance lines: transitions between ground state and first excited state. Opacity $\propto$ ion density and density of radiation field.

Hα: Transition between excited ionisation states. HII is the major ionisation stage for hydrogen in hot stars, can assume complete ionisation, and therefore $n_e \propto \rho$. Saha Equation for ionisation states $j, j+1$ and electronic state $\ell > 1$: $n_{\ell,j} \propto n_e n_{\ell,j+1} \propto \rho^2$.

The optical depth in the line is $\propto \alpha$, the absorption coefficient. $\alpha = n_{\rm H}\sigma \quad \propto n_e n_{\rm HII} \propto \rho^2$.

The MLR is given by $\dot{M} = 4\pi r^2 \rho v$, so $\alpha \propto \left(\frac{\dot{M}}{r^2 v}\right)^2$.

Compute optical depth from observed profile $\Longrightarrow$ estimate $\dot{M}$.